

Nanostructure and High Thermoelectric Performance in Nonstoichiometric AgPbSbTe Compounds: the Role of Ag

MIN ZHOU,^{1,2} JING-FENG LI,² HENG WANG,² TAKUJI KITA,³
LAIFENG LI,^{1,4} and ZHEN CHEN¹

1.—The Key Laboratory of Cryogenics, Technical Institute of Physics and Chemistry, Chinese Academy of Sciences, Beijing 100190, China. 2.—State Key Laboratory of New Ceramics and Fine Processing, Department of Materials Science and Engineering, Tsinghua University, Beijing 100084, China. 3.—Advanced Material Engineering Division, Vehicle Engineering Group, Higashifuji Technical Center, Toyota Motor Corporation, 1300, Mishuku, Susono, Shizuoka 410-1193, Japan. 4.—e-mail: laifengli@mail.ipc.ac.cn

High-performance nanostructured $\text{Ag}_{1-x}\text{Pb}_{22.5}\text{SbTe}_{20}$ thermoelectric materials have been fabricated using mechanical alloying and spark plasma sintering. A decrease in Ag content causes a great reduction in thermal conductivity and a prominent increase in ZT value. A minimum thermal conductivity of 0.86 W/m K and a high ZT value of 1.5 (700 K) have been obtained for the $\text{Ag}_{0.4}\text{Pb}_{22.5}\text{SbTe}_{20}$ sample. The smaller and denser nanoscopic regions with reduced Ag content are thought to enhance phonon scattering, resulting in decreased thermal conductivity and enhanced thermoelectric performance.

Key words: Thermoelectric materials, nanostructure, mechanical alloying, spark plasma sintering

INTRODUCTION

Thermoelectric (TE) materials are becoming increasingly important in the field of energy harvesting and conversion. The efficiency of TE devices is strongly associated with the dimensionless figure of merit (ZT), defined as $ZT = \alpha^2\sigma T/\kappa$, where α , σ , T , and κ are the Seebeck coefficient, the electrical conductivity, the absolute temperature, and the thermal conductivity, respectively.¹ In general, good TE materials have ZT values around unity. However, ZT values of up to 3 are considered to be essential for TE energy converters that can compete with mechanical power generation and active refrigeration. In the mid-1990s the milestone of $ZT \approx 1$ was exceeded and a high ZT value of 3 was reported.² For example, phonon-glass electron-crystal thermoelectric materials, such as skutterudites and clathrates,² were found to be good thermoelectric materials.^{2–5} In these compounds, the “rattling” motion of loosely bonded atoms within a large cage generates strong scattering against

lattice phonon propagation, but has less impact on the transport of electrons. As a consequence, the thermal conductivity of skutterudites and clathrates was greatly reduced while maintaining the electrical conductivity at a high level. In 2001, Venkatasubramanian et al.⁶ reported $\text{Bi}_2\text{Te}_3/\text{Sb}_2\text{Te}_3$ superlattices with a high ZT value of up to 2.4. Subsequently, Harman et al.⁷ reported $\text{PbTe}/\text{PbTeSe}$ quantum dot superlattices with a ZT value of higher than 3.0 at 600 K. For general applications, it is highly desired to develop high-performance bulk TE materials. In 2004, Hsu et al.⁸ reported $\text{AgPb}_m\text{SbTe}_{2+m}$ bulk TE materials with a high ZT value of 1.7 at 700 K fabricated by melting and slow cooling method. They showed that the nanoscopic inhomogeneities increased the phonon scattering and hence reduced the thermal conductivity. As a result, a high ZT value was obtained. Hsu et al. also reported the effect of chemical composition on the thermoelectric properties. For example, the electrical transport changed to *p*-type by doping Sn on the Pb sublattice or substituting Na for Ag in $\text{AgPb}_m\text{SbTe}_{2+m}$ materials. Maximum ZT values of 1.45 and 1.7 were obtained for *p*-type $\text{Ag}(\text{Pb}_{1-x}\text{Sn}_x)_m\text{SbTe}_{2+m}$ and $\text{Na}_{1-x}\text{Pb}_m\text{SbTe}_{2+m}$

materials, respectively.^{9,10} Kosuga et al. reported the effect of Ag and Pb content on the thermoelectric properties of $\text{Ag}_{1-x}\text{Pb}_{18+x}\text{SbTe}_{20}$ materials fabricated by melting and hot pressing methods.¹¹ Our previous work¹² revealed that the electrical transport behavior changed from *p*-type for $\text{Ag}_{0.8}\text{Pb}_{18}\text{SbTe}_{20}$ to *n*-type for Pb-rich $\text{Ag}_{0.8}\text{Pb}_{18+x}\text{SbTe}_{20}$ ($x \geq 3.5$) materials when extra Pb was added. A *ZT* value of 1.2 was obtained for a moderately Pb-rich $\text{Ag}_{0.8}\text{Pb}_{22.5}\text{SbTe}_{20}$ material, and then a higher *ZT* value of 1.5 was obtained by using a simple annealing treatment.¹³ The reason for such an increase in *ZT* value was that the number of nanoscopic inhomogeneities inside grains increased with annealing treatment. The Ag^+ and Sb^{3+} ions were inclined to form $\text{Ag}^+-\text{Sb}^{3+}$ pairs to maintain charge balance with the Te^{2-} for the $\text{Ag}_{0.8}\text{Pb}_{22.5}\text{SbTe}_{20}$ sample during annealing treatment. Such nanoscopic inhomogeneities enhanced phonon scattering, resulting in a reduction of thermal conductivity and increase of *ZT* value.

Our previous work also revealed that a powder metallurgy process combining mechanical alloying (MA) and spark plasma sintering (SPS) was suitable for fabricating $\text{AgPb}_m\text{SbTe}_{2+m}$ bulk materials, producing fine-grained materials with high *ZT* values.¹² In the present work, we fabricated $\text{Ag}_{1-x}\text{Pb}_{22.5}\text{SbTe}_{20}$ materials by using the MA and SPS method, and studied the role of Ag content in

the thermoelectric properties of the $\text{Ag}_{1-x}\text{Pb}_{22.5}\text{SbTe}_{20}$ materials. It was very interesting that a small decrease in Ag content greatly reduced the thermal conductivity and increased the thermoelectric properties. A high *ZT* value of 1.5 was obtained for the $\text{Ag}_{0.4}\text{Pb}_{22.5}\text{SbTe}_{20}$ sample, being 40% higher than that of the $\text{Ag}_{0.8}\text{Pb}_{22.5}\text{SbTe}_{20}$ sample with higher Ag content.

EXPERIMENTAL PROCEDURES

Commercial elemental powders of Ag (99.9%, powder), Pb (99.9%, powder), Sb (99.999%, powder), and Te (99.999%, powder) were used as starting materials. Mixtures of these powders were subjected to MA in a planetary ball mill (QM-2L) using hardened stainless-steel vials and balls. The weight ratio of balls to powder was kept at about 20:1, and the milling vial was purged and filled with Ar + 5 atm.% H₂ atmosphere to prevent powder oxidation during the milling process. MA was performed at 350 rpm for 4 h, and the MA-derived powders were consolidated by SPS at 673 K for 5 min under axial pressure of 50 MPa. The microstructures of all the samples were examined by transmission electron microscopy (field-emission TEM, JEOL-2011 and JEOL-2010). The Seebeck coefficient and electrical resistivity were measured using a Seebeck coefficient/electrical resistance

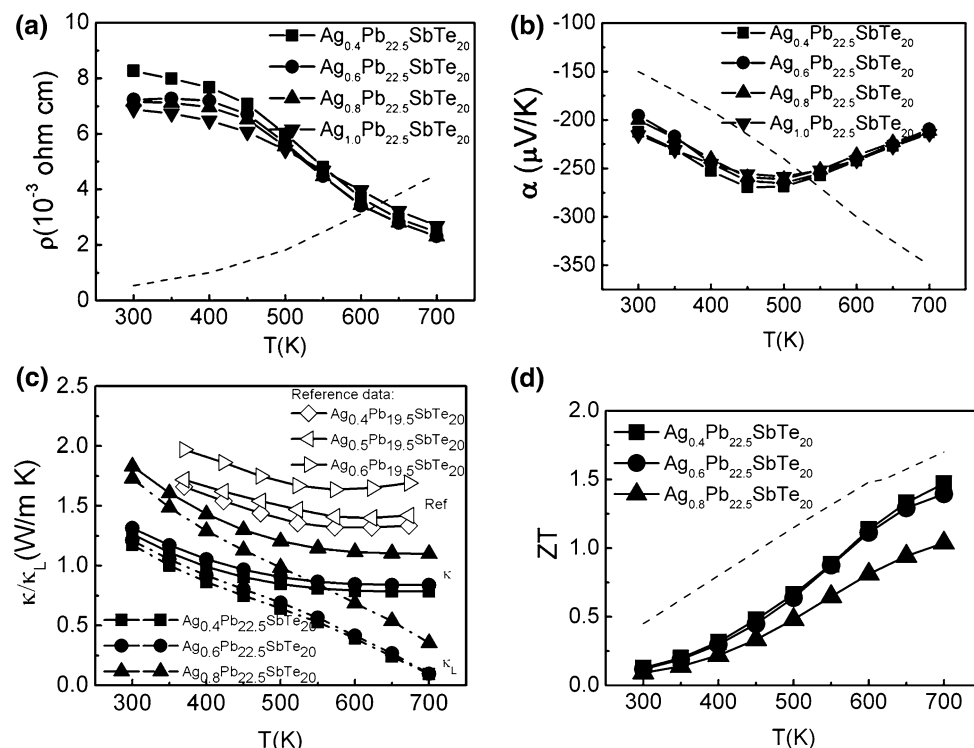


Fig. 1. Temperature dependence of (a) electrical resistivity, (b) Seebeck coefficient, (c) thermal conductivity, and (d) *ZT* values for the $\text{Ag}_{1-x}\text{Pb}_{22.5}\text{SbTe}_{20}$ ($0.2 \leq x \leq 0.6$) samples. The reference data in (c) is from Kosuga et al.¹¹ The dashed line in (a), (b), and (d) indicates the electrical resistivity, Seebeck coefficient, and *ZT* data reported by Hsu.⁸ The data for the $\text{Ag}_{0.8}\text{Pb}_{22.5}\text{SbTe}_{20}$ sample are reported in our previous work.¹¹

measuring system (ZEM-2). The thermal conductivity (κ) was calculated using the equation $\kappa = \lambda C_p d$, where λ is the thermal diffusivity, C_p is the heat capacity, and d is the bulk density of the sample, respectively. The thermal diffusivity was measured by a laser flash technique (NETZSCH LFA427). The heat capacity was measured using differential scanning calorimetry. The results were confirmed independently at two different testing centers.

RESULTS AND DISCUSSION

Figure 1a and b show the temperature dependence of the electrical resistivity and the Seebeck coefficient of the $\text{Ag}_{1-x}\text{Pb}_{22.5}\text{SbTe}_{20}$ ($0 \leq x \leq 0.6$) samples, respectively. The dashed line in the figures was extracted from the work of Hsu et al.⁸ The electrical resistivity of the $\text{AgPb}_{22.5}\text{SbTe}_{20}$ sample was on the order of $1.0 \times 10^{-3} \Omega \text{ cm}$ over the measured temperature range (300 K to 700 K). The electrical resistivity decreased with temperature, indicating semiconducting transport behavior, whereas Hsu et al. reported degenerate semiconducting transport behavior for $\text{AgPb}_m\text{SbTe}_{m+2}$. The

difference in transport behavior may be related to the carrier concentration. With decreasing Ag content, the electrical resistivity increased at around room temperature. This was similar to our previous work,¹² where the electrical resistivity increased with decreasing Pb content in association with a decrease of carrier concentration. The absolute value of the Seebeck coefficient $|\alpha|$ for the $\text{Ag}_{1-x}\text{Pb}_{22.5}\text{SbTe}_{20}$ ($0 \leq x \leq 0.6$) samples increased with temperature and reached a maximum at about 450 K to 500 K, but then started to decrease for temperature above 450 K to 500 K. The maximum $|\alpha|$ was $270 \mu\text{V/K}$ for $\text{Ag}_{0.4}\text{Pb}_{22.5}\text{SbTe}_{20}$ at 450 K. Below 450 K to 500 K, $|\alpha|$ increased with temperature, indicating that the conduction could be dominated by extrinsic charge carriers excited from impurity states. Above 450 K to 500 K, $|\alpha|$ decreased with temperature. The dip in the α versus T characteristic coincided with a “kink” in the ρ versus T curve around 500 K and could thus be attributed to hole-pair excitation across the energy gap.

Figure 1c shows the temperature dependence of the thermal conductivity of the $\text{Ag}_{1-x}\text{Pb}_{22.5}\text{SbTe}_{20}$ ($0.2 \leq x \leq 0.6$) samples. The thermal conductivities

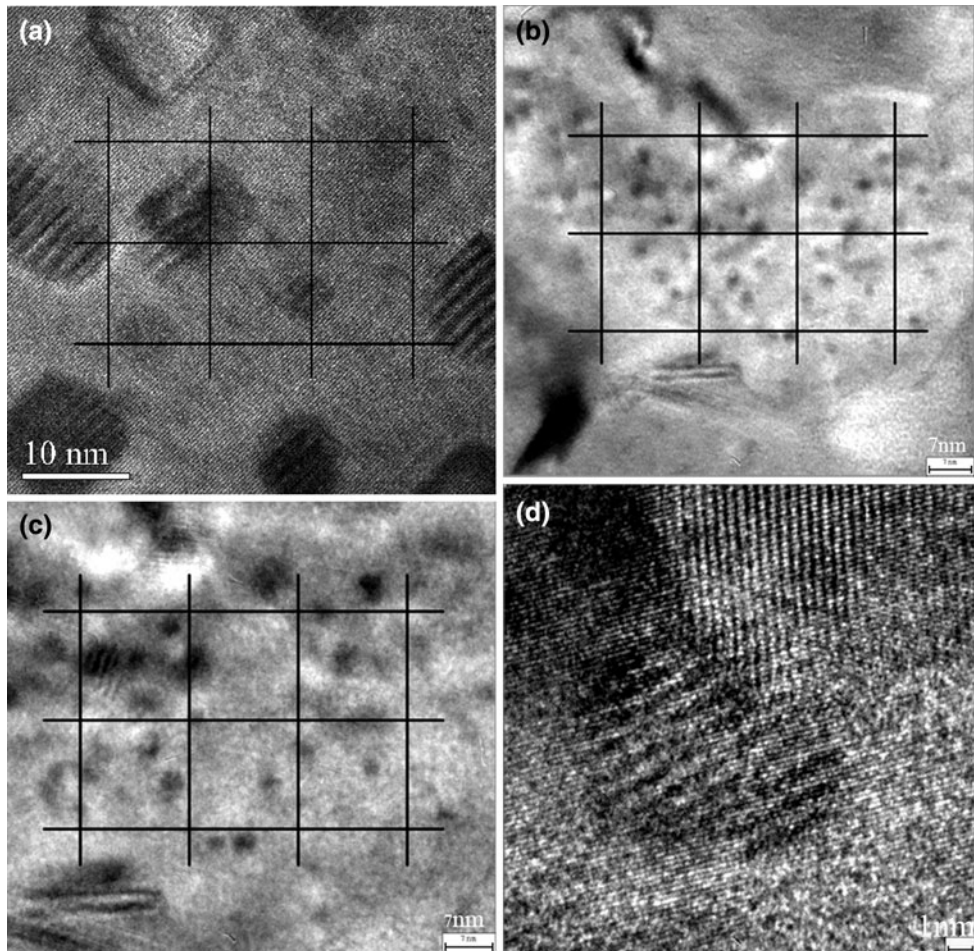


Fig. 2. TEM and HRTEM images of: $\text{Ag}_{1-x}\text{Pb}_{22.5}\text{SbTe}_{20}$ with (a) $x = 0.2$, (b) $x = 0.4$, and (c) $x = 0.6$ samples; and (d) $\text{Ag}_{0.6}\text{Pb}_{22.5}\text{SbTe}_{20}$ sample.

of all the samples decreased with temperature, which was mainly caused by increased phonon–phonon scattering at high temperatures. The thermal conductivity significantly decreased with decreasing Ag content, and a low thermal conductivity of 0.86 W/m K was obtained for the $\text{Ag}_{0.4}\text{Pb}_{22.5}\text{SbTe}_{20}$ sample in a wide temperature range of 550 K to 700 K. This value was just 70% of that of the $\text{Ag}_{0.8}\text{Pb}_{22.5}\text{SbTe}_{20}$ sample with a higher Ag content. Kosuga et al. reported a similar result in Ref. 11, where the thermal conductivity decreased with decreasing Ag content for $\text{Ag}_{1-x}\text{Pb}_{18+x}\text{SbTe}_{20}$ materials fabricated by melting and hot pressing method, as shown by open symbols in Fig. 1c, though the thermal conductivities were over 50% higher than our results.

Figure 1d shows the temperature dependence of the ZT values of the $\text{Ag}_{1-x}\text{Pb}_{22.5}\text{SbTe}_{20}$ ($0.2 \leq x \leq 0.6$) samples. The ZT values increased with decreasing Ag content. A maximum ZT value of 1.5 was obtained for the $\text{Ag}_{0.4}\text{Pb}_{22.5}\text{SbTe}_{20}$ sample at 700 K, being 40% higher than that of $\text{Ag}_{0.8}\text{Pb}_{22.5}\text{SbTe}_{20}$ with slightly higher Ag content at the same temperature. This value was very close to the maximum ZT value of 1.7 reported by Hsu et al.⁸ (dashed line in Fig. 1d). It is worth noting that the powder-based fabrication process combining MA and SPS method was simpler than that reported by Hsu et al.

It should be noted that a reduction in thermal conductivity and a great increase in ZT value were

observed with a small decrease in Ag content for the $\text{Ag}_{1-x}\text{Pb}_{22.5}\text{SbTe}_{20}$ materials. In our previous work,¹³ it was discussed that some Pb^{2+} sublattices were substituted by Ag^+ and Sb^{3+} ions and that Ag^+ and Sb^{3+} ions were inclined to form $\text{Ag}^+-\text{Sb}^{3+}$ pairs in the AgPbSbTe compound. Figure 2 shows some typical TEM and high-resolution transmission electron microscopy (HRTEM) images of Ag-poor $\text{Ag}_{1-x}\text{Pb}_{22.5}\text{SbTe}_{20}$ ($x = 0.2, 0.4, 0.6$) samples. We indeed observed a large quantity of nanoscopic black dots dispersed randomly inside grains in all samples. There were many nanoscopic regions with size of 5 nm to 10 nm inside all the crystal grains for the $\text{Ag}_{0.8}\text{Pb}_{22.5}\text{SbTe}_{20}$ sample, as shown in Fig. 2a. With decreasing Ag content, smaller and denser nanoscopic regions were observed inside crystal grains (Fig. 2b, c). Figure 2d shows a typical HRTEM image of the $\text{Ag}_{0.6}\text{Pb}_{22.5}\text{SbTe}_{20}$ sample, where the size of typical nanoscopic regions was about 1 nm to 5 nm. The HRTEM image also shows lots of localized wavy patterns that were embedded and dispersed inside the crystal grains. Squares were drawn on Fig. 2a–c to assess the density of nanoscopic regions in the crystal grains. Clearly, there were fewer than five nanoscopic regions in four grids (about 400 nm^2) for the $\text{Ag}_{0.8}\text{Pb}_{22.5}\text{SbTe}_{20}$ sample, as shown in Fig. 2a. With decreasing Ag content, more nanoscopic regions (> 20) were observed in four grids (about 400 nm^2) for the $\text{Ag}_{0.6}\text{Pb}_{22.5}\text{SbTe}_{20}$ and $\text{Ag}_{0.4}\text{Pb}_{22.5}\text{SbTe}_{20}$ samples, as shown in Fig. 2b and c, respectively. As discussed previously,¹² these nanoscopic regions

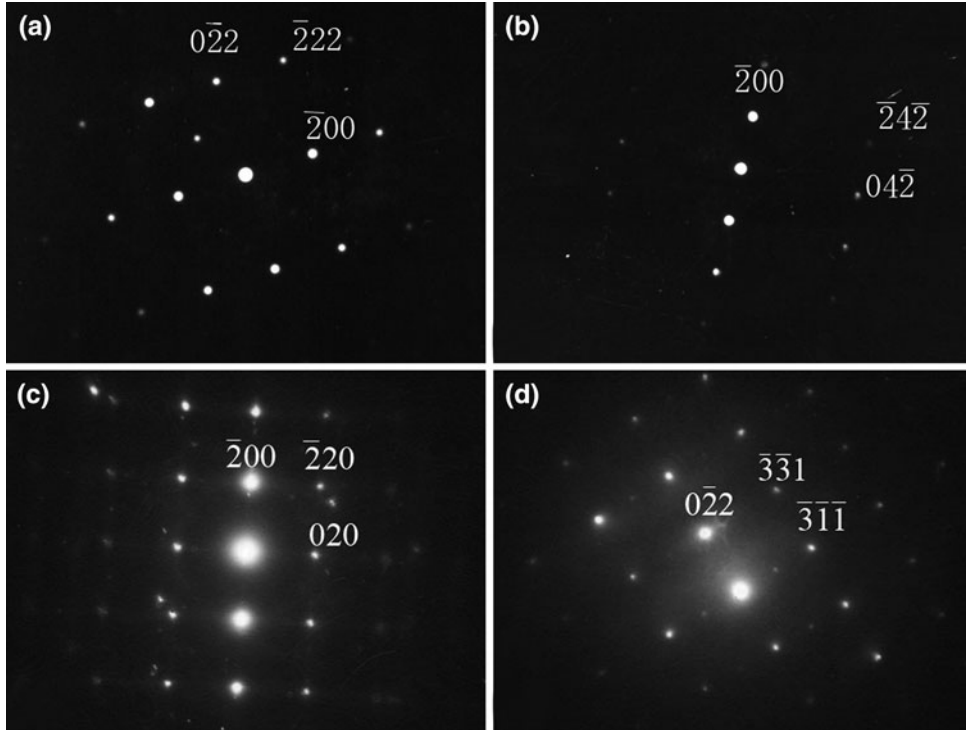


Fig. 3. Typical selected-area electron diffraction (SAED) patterns of $\text{Ag}_{0.8}\text{Pb}_{22.5}\text{SbTe}_{20}$ and $\text{Ag}_{0.6}\text{Pb}_{22.5}\text{SbTe}_{20}$ samples viewed along different directions: (a) [011] and (b) [013] of $\text{Ag}_{0.8}\text{Pb}_{22.5}\text{SbTe}_{20}$ sample, (c) [001] and (d) [$\bar{2}33$] of $\text{Ag}_{0.6}\text{Pb}_{22.5}\text{SbTe}_{20}$ sample. Splitting spots on the [001] zone axis (Fig. 2c) highlight multiphases with identical symmetry but different cell parameters.

were coherent with their surrounding crystal matrix. They should be Ag/Sb-rich regions embedded in the surrounding matrix endotaxially without disturbing the electronic flow. With decreasing Ag content, Ag⁺-Sb³⁺ pairs may be disturbed and excessive Pb is inclined to take some of the sublattice sites that would otherwise be occupied by Ag⁺-Sb³⁺ pairs. This may cause the smaller and denser nanoscopic regions, which are thought to enhance phonon scattering and decrease the thermal conductivity.

Figure 3 shows the electron diffraction figures of the Ag_{0.8}Pb_{22.5}SbTe₂₀ and Ag_{0.6}Pb_{22.5}SbTe₂₀ samples. Patterns exhibiting a perfect face-centered cubic (fcc) lattice (Fig. 3a, b, d) and sometimes accompanied by splitting spots (Fig. 3c) were observed. The patterns exhibiting splitting spots are evidence of the coexistence of two phases in the same area with similar but not identical cell parameters and identical crystallographic orientation. This observation strongly implies a well-defined compositional fluctuation in the Ag_{1-x}Pb_{22.5}SbTe₂₀ materials. The electron diffraction studies clearly showed that the Ag-poor Ag_{1-x}Pb_{22.5}SbTe₂₀ samples possessed different domains exhibiting nanostructures. The large number of nanoscopic regions and surrounding interfaces could provide a formidable barrier for phonon transmission, and thereby greatly decrease the thermal conductivity. Similar results were reported for PbTe and BiSbTe thermoelectric materials,¹⁴ where submicrometer grains and subsequently increased crystal boundaries were favorable for scattering of a wide spectrum of phonons.

CONCLUSIONS

We applied the MA and SPS technique to synthesize high-ZT polycrystalline bulk thermoelectric materials. The high ZT results mainly from low thermal conductivity due to increased phonon scattering from a high density of nanoscopic inhomogeneities and surrounding interfaces in the nanocomposite. The thermal conductivity was greatly reduced with decreasing Ag content, and a low thermal conductivity of 0.86 W/m K was obtained for the Ag-poor Ag_{0.4}Pb_{22.5}SbTe₂₀ sample in a wide temperature range of 550 K to 700 K. A peak

ZT value of 1.5 (at 700 K) was obtained for the Ag_{0.4}-Pb_{22.5}SbTe₂₀ sample, being 40% higher than that of the Ag_{0.8}Pb_{22.5}SbTe₂₀ sample with higher Ag content. The smaller and denser nanoscopic regions with decreasing Ag content are thought to enhance phonon scattering, resulting in decreased thermal conductivity and enhanced thermoelectric performance.

ACKNOWLEDGMENTS

The authors acknowledges financial support of the National Basic Research Program of China (Grant No. 2007CB607500), Tsinghua-Toyota collaborative research project (No. 0307J36), National Natural Science Foundation of China (No. 50802101, No. 50325207, and No. 50820145203), and Natural Science Foundation of Beijing (Grant No. 2072009).

REFERENCES

1. A.F. Loffe, *Semiconductor Thermoelements and Thermoelectric Cooling* (UK: Infosearch, 1957).
2. B.C. Sales, D. Mandrus, and R.K. Williams, *Science* 272, 1325 (1996).
3. G.S. Nolas, D.T. Morelli, and T.M. Tritt, *Annu. Rev. Mater. Sci.* 29, 89 (1999).
4. G.S. Nolas, J.L. Cohn, G.A. Slack, and S.B. Schujman, *Appl. Phys. Lett.* 73, 178 (1998).
5. G.A. Slack, *CRC Handbook of Thermoelectrics*, ed. D.M. Rowe (CRC Press, USA, 1995).
6. R. Venkatasubramanian, E. Siivola, V. Colpitts, and B. Quinn, *Nature* 413, 597 (2001).
7. T.C. Harman, P.J. Taylor, M.P. Walsh, and B.E. LaForge, *Science* 297, 2229 (2002).
8. K.F. Hsu, S. Loo, F. Guo, W. Chen, J.S. Dyck, C. Uher, T. Hogan, E.K. Polychroniadis, and M.G. Kanatzidis, *Science* 303, 818 (2004).
9. J. Androulakis, K.F. Hsu, R. Pcionek, H. Kong, C. Uher, J.J. D'Angelo, A. Downey, T. Hogan, and M.G. Kanatzidis, *Adv. Mater.* 18, 1170 (2006).
10. P.F.P. Poudeu, J. D'Angelo, A.D. Downey, J.L. Short, T.P. Hogan, and M.G. Kanatzidis, *Angew. Chem. Int. Ed.* 45, 3835 (2006).
11. A. Kosuga, M. Uno, K. Kurosaki, and S. Yamanaka, *J. Alloys Compd* 391, 288 (2005).
12. M. Zhou, J.-F. Li, and H. Wang, *Chin. Sci. Bull.* 52, 990 (2007).
13. M. Zhou, J.-F. Li, H. Wang, and T. Kita, *J. Am. Chem. Soc.* 130, 4527 (2008).
14. Y.C. Lan, B. Poudel, Y. Ma, D.Z. Wang, M.S. Dresselhaus, G. Chen, and Z.F. Ren, *Nano Lett.* 9, 1419 (2009).